Charge-Assisted Hydrogen Bonding and Other Noncovalent Interactions in the Self-Assembly of the Organometallic Building Block [(η^6-hydroquinone)Rh(P(OPh)$_3$)$_2$]$^+$ with a Range of Counteranions

Seung Uk Son,*[,†] Jeffrey A. Reingold,[‡] Gene B. Carpenter,[‡] Paul T. Czech,[§] and Dwight A. Sweigart*[,‡]

Departments of Chemistry, Sungkyunkwan University, Suwon 440-746, Korea, Brown University, Providence, Rhode Island 02912, and Providence College, Providence, Rhode Island 02918

Received May 19, 2006

The synthesis and X-ray structures are reported for [(η^6-hydroquinone)Rh(P(OPh)$_3$)$_2$]$^+$X$^-$ (X = BF_4, ClO_4, SbF_6, OTf, OTs, OPf), [(η^6-resorcinol)Rh(P(OPh)$_3$)$_2$]$^+$$BF_4^-$, and [($\eta^6$-4,4′-biphenol)Rh(P(OPh)$_3$)$_2$]$^+$$BF_4^-$. In these complexes, the −OH groups are activated by the electrophilic rhodium moiety to participate in charge-assisted hydrogen bonding to the anionic counterion. The crystal structures feature three kinds of noncovalent interactions—hydrogen bonding, Coulombic attraction, and $\pi-\pi$ stacking, which result in an intriguing array of architectures: dimeric, 1-D chain, C_2 helical, and C_3 helical. The nature of the charge-assisted hydrogen bonding and the resulting 3-D structure in these systems are remarkably dependent on the identity of the anion. Robust porous networks are formed rapidly (minutes or less) with [(η^6-hydroquinone)Rh(P(OPh)$_3$)$_2$]$^+$X$^-$ (X = BF_4, ClO_4) and [(η^6-resorcinol)Rh(P(OPh)$_3$)$_2$]$^+$$BF_4^-$. The hydrophobic pores in [(η^6-hydroquinone)Rh(P(OPh)$_3$)$_2$]$^+$$ClO_4^-$ bind toluene reversibly. This work demonstrates that self-assembly of well-designed organometallic building blocks via charge-assisted hydrogen bonding is an effective strategy for the construction of robust porous networks. With counterions containing both oxygen and fluorine, it was found that the former is invariably the hydrogen bond acceptor, a result in agreement with atomic charge calculations. It is anticipated that self-assembly via charge-assisted hydrogen bonding is an approach applicable in many organometallic systems.

Introduction

The self-assembly of molecules or molecular units into supramolecular arrays can be driven by covalent bond formation and/or can be driven by noncovalent interactions such as $\pi-\pi$ stacking, hydrogen bonding, and van der Waals forces.[1] Hydrogen bonding has been recognized as a particularly powerful tool in this regard because of its unique directionality and specificity.[2,3] Supramolecular assemblies predicated on hydrogen bonding can be reinforced by the cooperative action of multipoint H bonds or additional cooperative interactions between the modular components of the assembly.[2a,4] An important example of this is so-called *charge-assisted* hydrogen bonding, which can occur in ionic or zwitterionic systems and refers to hydrogen bonding accompanied by Coulombic interactions resulting from the inherent electronic charges.[5] This can lead to an exceptionally strong interaction between the oppositely charged components. For example, depending on the identity of the anionic component,[6] guanidinium cations can have a cation−anion association constant as high as 10^6 M^{-1}. Similarly, charge-assisted hydrogen bonding can be an effective strategy for fully utilizing the directional properties of hydrogen-bonding-mediated assembly in organometallic systems.[7,8]

* To whom correspondence should be addressed. E-mail: sson@skku.edu (S.U.S.); dwight_sweigart@brown.edu (D.A.S.).

† Sungkyunkwan University.

‡ Brown University.

§ Providence College.

(1) (a) Lehn, J.-M. *Supramolecular Chemistry: Concepts and Perspectives*; VCH: Weinheim, Germany, 1995. (b) Conn, M. M.; Rebek, J., Jr. *Chem. Rev.* **1997**, *97*, 1647. (c) Fyfe, M. C. T.; Stoddart, J. F. *Acc. Chem. Res.* **1997**, *30*, 393. (d) Bowden, N. B.; Weck, M.; Choi, I. S.; Whitesides, G. M. *Acc. Chem. Res.* **2001**, *34*, 231. (e) Malek, N.; Maris, T.; Perron, M.-E.; Wuest, J. D. *Angew. Chem., Int. Ed.* **2005**, *44*, 4021. (f) Hunter, C. A.; Lawson, K. R.; Perkins, J.; Urch, C. J. *J. Chem. Soc., Perkin Trans. 2* **2001**, 651.

(2) (a) Prins, L. J.; Reinhoudt, D. N.; Timmerman, P. *Angew. Chem., Int. Ed.* **2001**, *40*, 2382. (b) Etter, M. C. *Acc. Chem. Res.* **1990**, *23*, 120. (c) Fredericks, J. R.; Hamilton, A. D. In *Comprehensive Supramolecular Chemistry*; Sauvage, J.-P., Hosseini, M. W., Eds.; Pergamon Press: Oxford, U.K., 1996; Vol. IX, Chapter 16.

(3) (a) Beatty, A. M. *Coord. Chem. Rev.* **2003**, *246*, 131. (b) Adachi, K.; Sugiyama, Y.; Yoneda, K.; Yamada, K.; Nozaki, K.; Fuyuhiro, A.; Kawata, *Chem. Eur. J.* **2005**, *11*, 6616.

(4) For representative examples see: (a) Nadin, A.; Derrer, S.; McGeary, R. P.; Goodman, J. M.; Raithby, P. R.; Holmes, A. B. *J. Am. Chem. Soc.* **1995**, *117*, 9768. (b) Bisson, A. P.; Hunter, C. A. *Chem. Commun.* **1996**, 1723. (c) Adams, H.; Carver, F. J.; Hunter, C. A.; Morales, J. C.; Seward, E. M. *Angew. Chem., Int. Ed. Engl.* **1996**, *35*, 1542. (d) Corbin, P. S.; Zimmerman, S. C. *J. Am. Chem. Soc.* **2000**, *122*, 3779.

(5) Ward, M. D. *Chem. Commun.* **2005**, 5838.

(6) (a) Schmidtchen, F. P.; Berger, M. *Chem. Rev.* **1997**, *97*, 1609. (b) Schmuck, C. *Eur. J. Org. Chem.* **1999**, *2397*, 7. (c) Nelen, M. I.; Eliseev, A. V. *J. Chem. Soc., Perkin Trans. 2* **1997**, 1359. (d) Linton, B.; Hamilton, A. D. *Tetrahedron* **1999**, *55*, 6027. (e) Russell, V. A.; Etter, M. C.; Ward, M. D. *J. Am. Chem. Soc.* **1994**, *116*, 1941. (f) Dixon, R. P.; Geib, S. J.; Hamilton, A. D. *J. Am. Chem. Soc.* **1992**, *114*, 365. (g) Schrader, T. *Chem. Eur. J.* **1997**, *3*, 1537. (h) Schellhaas, K.; Schmalz, H.-G.; Bats, J. W. *Chem. Eur. J.* **1998**, *4*, 57. (i) Schmuck, C. *Chem. Commun.* **1999**, 843.

(7) (a) Braga, D.; Maini, L.; Grepioni, F. *Organometallics* **2001**, *20*, 1875. (b) Braga, D.; Cojazzi, G.; Emiliani, D.; Maini, L.; Grepioni, F. *Organometallics* **2002**, *21*, 1315. (c) Braga, D.; Polito, M.; D'Addario, D.; Tagliavini, E.; Proserpio, D. M.; Grepioni, F.; Steed, J. W. *Organometallics* **2003**, *22*, 4532. (d) Braga, D.; Polito, M.; Bracaccini, M.; D'Addario, D.; Tagliavini, E.; Sturba, L. *Organometallics* **2003**, *22*, 2142. (e) Braga, D.; Polito, M.; D'Addario, D.; Grepioni, F. *Cryst. Growth Des.* **2004**, *4*, 1109. (f) Braga, D.; Polito, M.; Grepioni, F. *Cryst. Growth Des.* **2004**, *4*, 769.

(8) Braga, D.; Grepioni, F. *Acc. Chem. Res.* **2000**, *33*, 601.

10.1021/om0604425 CCC: $33.50
Publication on Web 09/26/2006

Chart 1. Organometallic Building Blocks Utilized in This Study

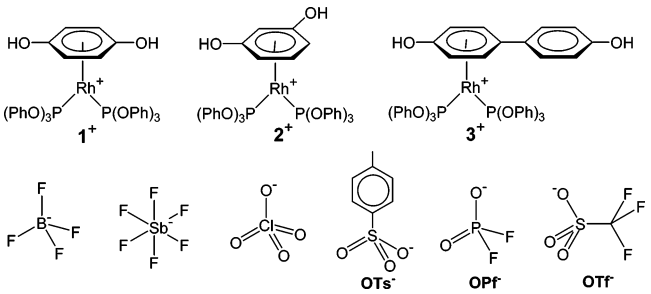

Recently, it has been recognized that the structural and chemical versatility of *organometallic* building blocks can be utilized to prepare supramolecular assemblies with distinct physical and chemical properties that cannot be replicated in purely organic systems.[9,10] For example, self-assembled coordination networks that feature transition-metal nodes and the anionic complex [(η^4-quinone)Mn(CO)$_3$]$^-$ as organometallo-ligand spacers have been extensively reported.[10] In addition to coordination-mediated self-assembly, there has been a considerable interest in supramolecular organometallic assemblies formed via noncovalent interactions. Braga and co-workers, for example, have described the self-assembly of a variety of organometallic sandwich compounds through charge-assisted hydrogen bonding.[7,8] We reported[11] a polymeric network derived from charge-assisted hydrogen bonding between [(η^6-1,4-hydroquinone)Mn(CO)$_3$]$^+$ and SiF_6^{2-} and more recently communicated preliminary results for the formation of related networks resulting from interactions between the −OH groups in [(η^6-1,4-hydroquinone)Rh(P(OPh)$_3$)$_2$]$^+$ (**1**$^+$) and [(η^6-1,3-hydroquinone)Rh(P(OPh)$_3$)$_2$]$^+$ (**2**$^+$) with the BF_4^- counteranion.[12] In the latter case, the assembly resulted in the formation of porous materials containing interesting hydrophobic channels that consist entirely of phenyl groups from the triphenyl phosphite ligands.

Herein we report a comprehensive study of noncovalent self-assembly in the ionic η^6-hydroxybenzene complexes illustrated in Chart 1. These organometallic salts were found to exhibit differential hydrogen-bonding and $\pi-\pi$ stacking interactions, resulting in an intriguing array of both discrete and polymeric supramolecular solid-state structures. Solution-phase IR studies and molecular orbital calculations of atomic charges are presented to rationalize the structural variations found.

Results and Discussion

Synthesis of η^6-Hydroxybenzene Rhodium Salts. The complexes [**2**]BF_4 and [**3**]BF_4 were synthesized in good yields

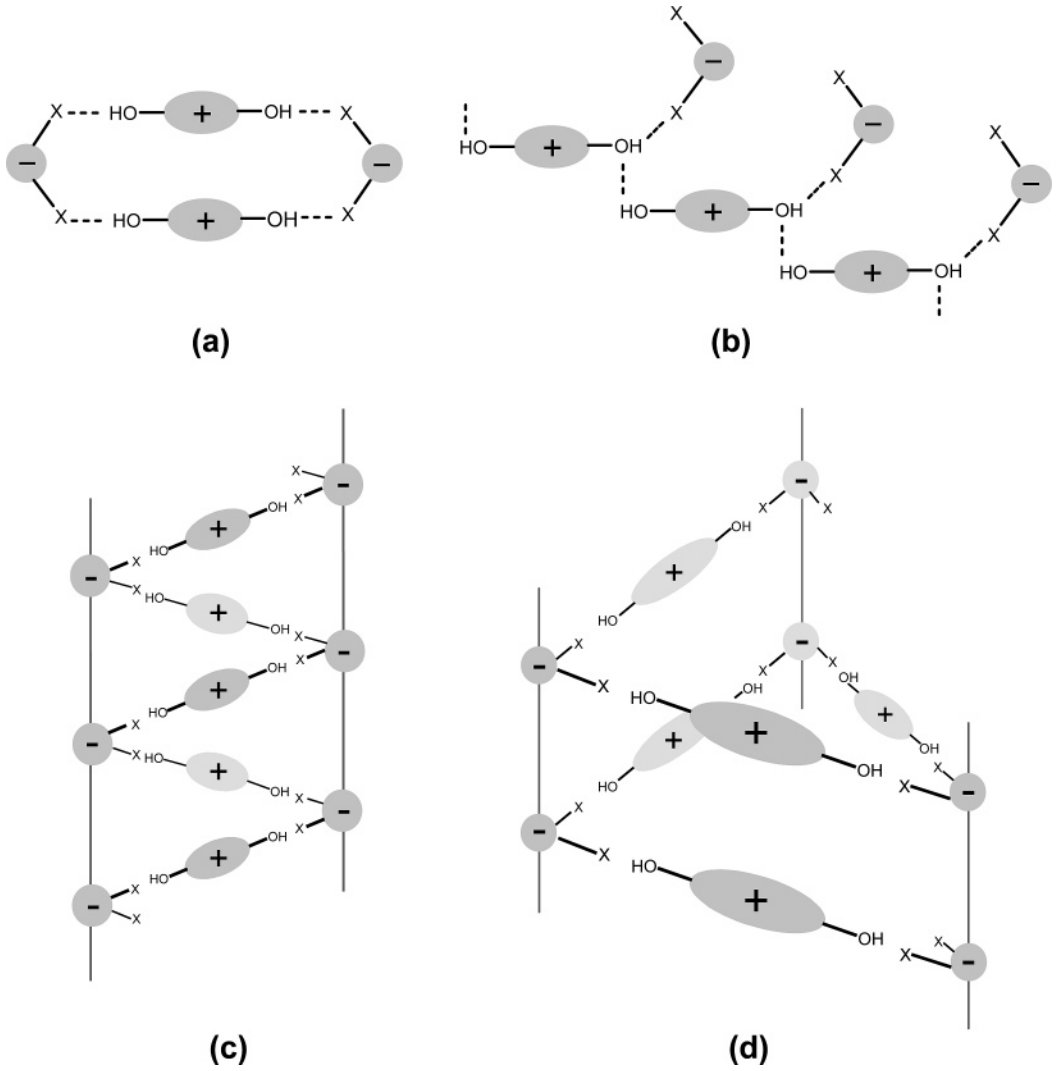

Figure 1. Hydrogen-bonded structural patterns found in the solid state for [**1**$^+$−**3**$^+$]X$^-$: (a) dimeric; (b) 1-D chain; (c) C_2 helical; (d) C_3 helical.

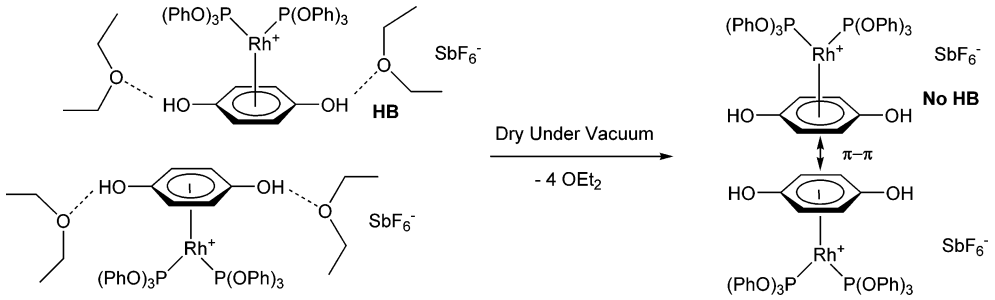

Figure 2. Hydrogen-bonded structure of crystalline $\mathbf{1}^{+}SbF_6^{-}$ as a diethyl ether solvate (left) and slippage to a $\pi-\pi$-stacked structure upon drying (right).

Table 1. Crystallographic Data

	$\mathbf{1}^{+}SbF_6^{-}$	$\mathbf{1}^{+}SbF_6^{-}$(hex)	$\mathbf{1}^{+}OTf^{-}$	$\mathbf{1}^{+}OPf^{-}$	$\mathbf{3}^{+}BF_4^{-}$	$\mathbf{1}^{+}OTs^{-}$	$\mathbf{1}^{+}ClO_4^{-}$
formula	$C_{50}H_{56}F_6O_{10}P_2RhSb$	$C_{42}H_{36}F_6O_8P_2RhSb$	$C_{44}H_{38}Cl_2F_3O_{11}P_2RhSb$	$C_{42}H_{36}F_2O_{10}P_3Rh$	$C_{48}H_{40}BF_4O_8P_2Rh$	$C_{50}H_{45}Cl_2O_{11}P_2RhS$	$C_{42}H_{36}ClO_{12}P_2Rh$
fw	1217.55	1069.31	1067.55	934.53	996.46	1089.67	933.01
T, K	100(2)	173(2)	100(2)	100(2)	100(2)	293(2)	100(2)
cryst syst	triclinic	triclinic	triclinic	triclinic	monoclinic	orthorhombic	rhombohedral
space group	$P\bar{1}$	$P\bar{1}$	$P\bar{1}$	$P\bar{1}$	$P2/c$	$P2_12_12_1$	$R\bar{3}$
a, Å	12.834(1)	10.669(2)	10.597(1)	10.843(1)	17.960(5)	11.875(3)	38.625(2)
b, Å	13.259(1)	14.186(3)	13.952(1)	11.245(1)	11.306(3)	17.555(5)	38.625(2)
c, Å	17.158(1)	16.885(3)	16.587(1)	17.908(1)	23.267(7)	24.061(7)	15.096(1)
α, deg	94.600(1)	65.795(4)	74.722(1)	105.394(1)	90	90	90
β, deg	99.863(1)	85.774(4)	84.604(2)	90.398(1)	105.502(5)	90	90
γ, deg	116.234(1)	70.863(4)	70.769(1)	107.279(1)	90	90	120
V, Å^3	2539.9(3)	2196.5(7)	2233.7(3)	2001.5(3)	4553(2)	5016(3)	19505(1)
Z	2	2	2	2	4	4	18
D_{calcd}, g/cm^3	1.592	1.617	1.587	1.551	1.454	1.443	1.430
F(000)	1232	1064	1084	952	2032	2232	8568
cryst size, mm	0.17 × 0.16 × 0.15	0.15 × 0.11 × 0.05	0.10 × 0.09 × 0.05	0.07 × 0.06 × 0.05	0.14 × 0.14 × 0.10	0.14 × 0.11 × 0.04	0.12 × 0.11 × 0.10
θ range, deg	1.74−28.42	1.65−25.11	1.60−26.45	1.98−26.55	1.82−23.25	1.44−25.07	1.48−25.10
no. of rflns collected	30 290	21 333	24 103	21 442	35 882	47 263	63 011
no. of data/restraints/params	12 161/6/635	7778/0/505	9123/46/572	8253/0/513	6529/730/618	8890/0/606	7711/0/523
goodness of fit on F^2	1.026	1.022	1.128	1.076	1.067	0.930	1.030
final R indices ($I > 2\sigma(I)$)							
R1	0.0377	0.0943	0.0748	0.0725	0.1212	0.078	0.0789
wR2	0.0808	0.2578	0.1251	0.1558	0.2917	0.1451	0.2199

by treatment of the precursor $[Rh(P(OPh)_3)_2Cl]_2$[13] with $AgBF_4$ in methylene chloride to generate $[Rh(P(OPh)_3)_2]^{+}$ in situ, which was then reacted with resorcinol and 4,4′-biphenol, respectively. The 1,4-hydroquinone salts [**1**]X ($X^{-} = BF_4^{-}$, SbF_6^{-}, PF_6^{-}, ClO_4^{-},OTs^{-}, OTf^{-}) were synthesized in a similar manner, with the anion X^{-} deriving from the silver salt (AgX) utilized. Reactions utilizing silver nitrate and silver sulfate were unsuccessful, as were attempts to coordinate 1,3,5-trihydroxybenzene and 1,2,4-trihydroxybenzene.

As indicated in Chart 1, complexes $\mathbf{1}^{+}-\mathbf{3}^{+}$ present a number of noncovalent interaction sites: hydroxyl groups, F and O atoms in the counteranions, phenyl rings, and electronic charges. Consequently, organometallic crystal engineering using these building blocks may be expected to feature at least three kinds of noncovalent interactions: hydrogen bonding, Coulombic attraction, and $\pi-\pi$ stacking.

Solid-State Structures and Self-Assembly. Diagrams of the different types of solid-state structural patterns found in this study are shown in Figure 1. The cationic hydroxybenzene complexes ($\mathbf{1}^{+}-\mathbf{3}^{+}$) and the anionic companion (X^{-}) can assemble to generate dimeric, 1-D chain, C_2-helical, and C_3-helical motifs, most of which feature charge-assisted hydrogen bonding. Relevant X-ray crystallographic data are summarized in Table 1.

Crystals of $[(\eta^6$-1,4-hydroquinone$)Rh(P(OPh)_3)_2]^{+}SbF_6^{-}$ ($\mathbf{1}^{+}SbF_6^{-}$) suitable for single-crystal X-ray analysis were prepared by layering a methylene chloride solution at −20 °C with diethyl ether or hexane. Cube-shaped orange crystals and plate-shaped yellow crystals were obtained with diethyl ether and hexane cosolvents, respectively. The X-ray structure of the orange crystals revealed that the hydroquinone −OH groups are hydrogen-bonded to diethyl ether present in the crystal lattice (O···O = 2.6 Å), as shown in Figure 2 (left). The hydroquinone rings are arranged in pairs due to an edge-to-edge $\pi-\pi$ stacking interaction involving two carbon atoms of each ring. The average C···C contact between the edges of adjacent rings is 3.3 Å.

The simulated powder XRD pattern of $\mathbf{1}^{+}SbF_6^{-}\cdot 2Et_2O$ is shown in Figure 3a. The solid was found to slowly lose the incorporated solvent molecules. After the solid was dried under

(9) (a) Braga, D.; Grepioni, F.; Desiraju, G. R. *Chem. Rev.* **1998**, *98*, 1375. (b) Burrows, A. D.; Chan, C.-W.; Chowdhry, M. M.; McGrady, J. E.; Mingos, D. M. P. *Chem. Soc. Rev.* **1995**, *24*, 329. (c) Sun, S.-S.; Lees, A. J. *Inorg. Chem.* **2001**, *40*, 3154. (d) Kuehl, C. J.; Yamamoto, T.; Seidel, S. R.; Stang, P. J. *Org. Lett.* **2002**, *4*, 913. (e) Shin, D. M.; Chung, Y. K.; Lee, I. S. *Cryst. Growth Des.* **2002**, *2*, 493. (f) Kim, Y.; Verkade, J. G. *Inorg. Chem.* **2003**, *42*, 4262. (g) Hartnell, R. D.; Arnold, D. P. *Organometallics* **2004**, *23*, 391. (h) Dong, Y.-B.; Geng, Y.; Ma, J.-P.; Huang, R.-Q. *Inorg. Chem.* **2005**, *44*, 1693.

(10) (a) Oh, M.; Carpenter, G. B.; Sweigart, D. A. *Acc. Chem. Res.* **2004**, *37*, 1. (b) Reingold, J. A.; Son, S. U.; Kim, S. B.; Dullaghan, C. A.; Oh, M.; Frake, P. C.; Carpenter, G. B.; Sweigart, D. A. *Dalton Trans.* **2006**, 2385.

(11) Sun, S.; Carpenter, G. B.; Sweigart, D. A. *J. Organomet. Chem.* **1996**, *512*, 257.

(12) Son, S. U.; Reingold, J. A.; Carpenter, G. B.; Sweigart, D. A. *Chem. Commun.* **2006**, 708.

(13) Haines, L. M. *Inorg. Chem.* **1970**, *19*, 1517.

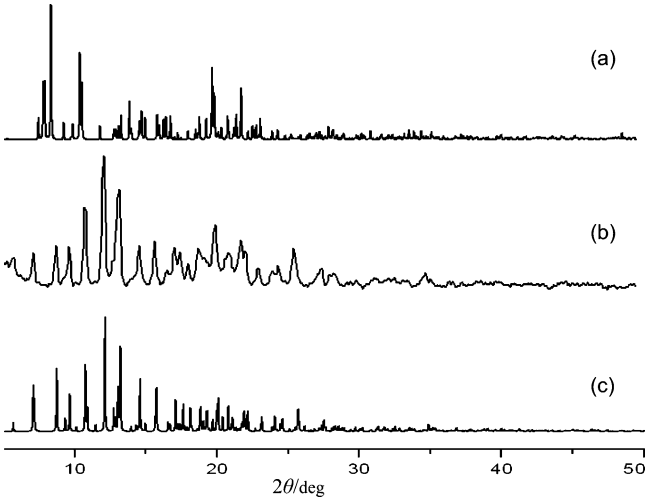

Figure 3. PX-RD patterns: (a) simulated pattern of $\mathbf{1}^{+}SbF_6^{-}\cdot 2Et_2O$ from single-crystal data; (b) pattern of $\mathbf{1}^{+}SbF_6^{-}$ crystals after drying under vacuum; (c) simulated pattern from single-crystal data of $\mathbf{1}^{+}SbF_6^{-}$ grown in CH_2Cl_2 and hexane.

vacuum for 1 day, the PXRD pattern changed significantly to that shown in Figure 3b, from which it is inferred that the solid remains crystalline but undergoes a substantial structural change upon solvent loss. It proved possible to ascertain the nature of this change, because the simulated PXRD obtained from single-crystal data for $\mathbf{1}^{+}SbF_6^{-}$ grown with hexane cosolvent (yellow plates) matched that obtained after drying $\mathbf{1}^{+}SbF_6^{-}\cdot 2Et_2O$ (compare parts c and b of Figure 3), suggesting that they have the same structure. The structure of the former, shown in Figure 2 (right), reveals a $\pi-\pi$-stacked dimeric aggregate with nearly eclipsed hydroquinone rings that are separated by an average of 3.5 Å and not involved in any hydrogen bonding. It is concluded that, upon drying, $\mathbf{1}^{+}SbF_6^{-}\cdot 2Et_2O$ undergoes a remarkable concerted hydroquinone ring slippage of ca. 3 Å with concomitant loss of hydrogen bonding to the ether and gain of $\pi-\pi$ stacking interactions, *all without the loss of crystallinity*.

Crystals of the triflate salt $\mathbf{1}^{+}OTf^{-}$ were grown by layering hexane on a methylene chloride solution at −20 °C. The solid-state structure consists of the dimeric unit illustrated in Figure 4 and follows the general pattern depicted in Figure 1a. The two hydroquinone rings are $\pi-\pi$ stacked (3.6 Å), and the −OH groups are hydrogen-bonded to the sulfonate oxygens of the triflate anion (average O···O = 2.68 Å). Since the sulfonate end of the triflate anion contains most of the net negative charge (vide infra), the hydrogen bonding would be expected to involve the oxygens rather than the fluorines and may be classified as charge-assisted. Analogous charge-assisted hydrogen bonding to the oxygen atoms in triflate has been reported to occur in $[Cp_2Ta(OH)_2][OTf^{-}]$.[14]

The synthesis of $\mathbf{1}^{+}PF_6^{-}$, with $AgPF_6$ as the anion source, proceeded smoothly and gave a product with a satisfactory elemental analysis. After slow recrystallization from methylene chloride, however, it became evident from subsequent single-crystal X-ray analysis and altered bulk elemental analysis that hydrolysis of the anion to $PF_2O_2^{-}$ (OPf^{-}) had occurred during the recrystallization process. The hydrolysis reaction probably stems from trace water and may have been accelerated by the acidic nature of the coordinated hydroquinone. Hydrolysis of PF_6^{-} in this manner has been observed previously.[15] The X-ray structure of $\mathbf{1}^{+}OPf^{-}$ (Figure 5) is very similar to that found for $\mathbf{1}^{+}OTf^{-}$. Charge-assisted hydrogen-bonding and $\pi-\pi$-stacking (3.5 Å) interactions dominate the observed dimeric units. Careful analysis of the X-ray data confirmed that the hydrogen bonding from the hydroquinone −OH groups is to oxygen and not fluorine acceptors on the OPf^{-} anion (average O···O = 2.65 Å).

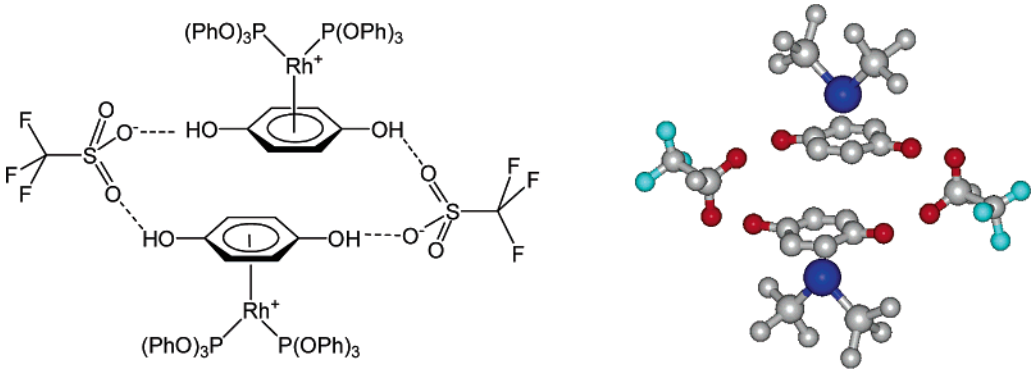

Figure 4. Dimeric structure of $\mathbf{1}^{+}OTf^{-}$, which features charge-assisted hydrogen-bonding and $\pi-\pi$-stacking interactions.

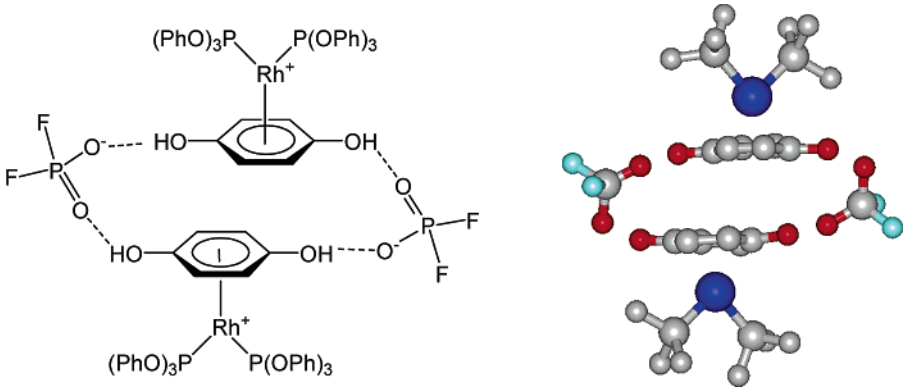

Figure 5. Dimeric structure of $\mathbf{1}^{+}OPf^{-}$ (compare to $\mathbf{1}^{+}OTf^{-}$ in Figure 4).

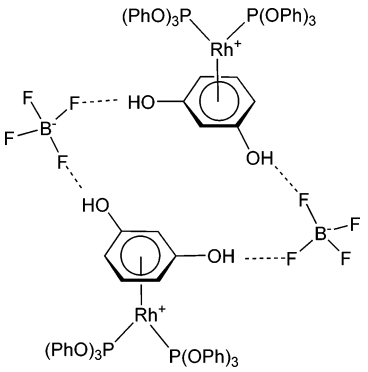

Figure 6. Dimeric structure of $\mathbf{2}^{+}BF_4^{-}$, which does not have $\pi-\pi$ interactions.

The dimeric structures found for $\mathbf{1}^{+}OPf^{-}$ and $\mathbf{1}^{+}OTf^{-}$ combine in a cooperative manner three types of noncovalent interactions: charge pairing, hydrogen bonding, and $\pi-\pi$ stacking. Interestingly, a different type of dimeric assembly was found for $[(\eta^6\text{-}1,3\text{-hydroquinone})Rh(P(OPh)_3)_2]^{+}BF_4^{-}$ ($\mathbf{2}^{+}BF_4^{-}$).[16] In this case, the dimer is held together by charge-assisted hydrogen bonding but geometric restrictions prevent $\pi-\pi$ stacking between the 1,3-hydroquinone rings (Figure 6). The hydrogen bond distances in $\mathbf{2}^{+}BF_4^{-}$ average O···F = 2.8 Å.

$[(\eta^6\text{-}4,4'\text{-biphenol})Rh(P(OPh)_3)_2]^{+}BF_4^{-}$ ($\mathbf{3}^{+}BF_4^{-}$) forms the hydrogen-bonding network depicted in Figure 1b. Only one F atom in the BF_4^{-} anion participates in hydrogen bond formation with the phenolic −OH groups. A 1-D polymeric chain structure results, shown in Figure 7a, with the hydrogen bond distances O···F = 2.6 Å and O···O = 2.7 Å. The 3-D crystal structure features small channels which are lined with phenyl groups from the triphenyl phosphite ligands that undergo $\pi-\pi$ stacking. The channels were found to be filled with unidentified disordered solvent molecules, which were located using PLATON software (Figure 7b).

The interesting C_2-helical chain motif shown in Figure 1c was found for the tosylate salt of $[(\eta^6\text{-}1,4\text{-hydroquinone})Rh(P(OPh)_3)_2]^{+}$ ($\mathbf{1}^{+}OTs^{-}$).[17] Long rod-shaped single crystals of $\mathbf{1}^{+}OTs^{-}$ were grown by layering a methylene chloride solution with hexane at −20 °C. The helical hydrogen-bonding network has C_2 projection symmetry (Figure 8). The space group ($P2_12_12_1$) implies the generation of chirality during the crystallization process, which means that the helices pack such that all possess the same direction of rotation (the Flack parameter for the structure shown was determined as −0.09(8)). The two independent hydrogen bonds in $\mathbf{1}^{+}OTs^{-}$ have O···O = 2.47 and 2.63 Å.

Single crystals of $\mathbf{1}^{+}BF_4^{-}$ and $\mathbf{1}^{+}ClO_4^{-}$ were grown by layering a methylene chloride solution with diethyl ether.[12] These two salts have virtually identical structures, which feature the intriguing C_3-helical hydrogen-bonded network shown in Figure 1d. Structural details for $\mathbf{1}^{+}ClO_4^{-}$ are shown in Figure 9. The hydrogen-bonding distances in $\mathbf{1}^{+}BF_4^{-}$ are F···O = 2.47, 2.60 Å, and those in $\mathbf{1}^{+}ClO_4^{-}$ are O···O = 2.38, 2.88 Å. In each compound, six C_3 helices assemble to generate the hexagonal channels or pores illustrated in Figure 10. The structure belongs to the centrosymmetric space group $R\bar{3}$, and the direction of rotation of the helices alternates around the channels. The channels themselves located at the core of the six helices consist of hydrophobic phosphite phenyl groups (Figure 10). Two of the three phenyl groups from each $P(OPh)_3$ ligand contribute to the channels, which have a diameter of ca. 10.5 Å and are separated by ca. 23 Å.

The ease of formation of the pore structure shown in Figure 10b for $\mathbf{1}^{+}ClO_4^{-}$ and $\mathbf{1}^{+}BF_4$ was investigated by comparing the PXRD pattern of slowly grown macrocrystals with that found for microcrystals obtained by rapid precipitation. The addition of diethyl ether to a methylene chloride solution of $\mathbf{1}^{+}ClO_4^{-}$ led to rapid precipitation of a powder that appeared under a microscope to consist of good-quality microcrystals. Relevant PXRD patterns for various samples of $\mathbf{1}^{+}ClO_4^{-}$ are shown in Figure 11a−c. The powder pattern simulated from single-crystal X-ray data is given in Figure 11a. The *actual* pattern obtained with well-formed macrocrystals of $\mathbf{1}^{+}ClO_4^{-}$ is very similar (Figure 11b). Interestingly, the PXRD of microcrystalline $\mathbf{1}^{+}ClO_4^{-}$ formed by simple rapid precipitation is similar (Figure 11c), indicating that precipitated $\mathbf{1}^{+}ClO_4^{-}$ is (i) indeed crystalline and (ii) has the same porous structure possessed by slowly grown single crystals (Figure 10). We come to the significant conclusion that the dynamic processes occurring in the assembly of the organometallic building block $\mathbf{1}^{+}ClO_4^{-}$ into an intricate 3-D supramolecular architecture with hexagonal channels operate on a fast preparative time scale. Thus, the synthesis of crystalline porous materials such as $\mathbf{1}^{+}ClO_4^{-}$ can be accomplished within seconds (precipitation) rather than requiring days (slow single-crystal growth).

Analogous conclusions obtain for the $\mathbf{1}^{+}BF_4^{-}$ analogue (Figure 11d−f), although, due to contamination by an unidentified species (asterisks in Figure 11e,f), the PXRD patterns are not as clear-cut as that seen with $\mathbf{1}^{+}ClO_4$. Stronger hydrogen bonding in $\mathbf{1}^{+}ClO_4^{-}$ compared to that in $\mathbf{1}^{+}BF_4^{-}$ (vide infra) may be responsible for a cleaner crystallization process with the former.

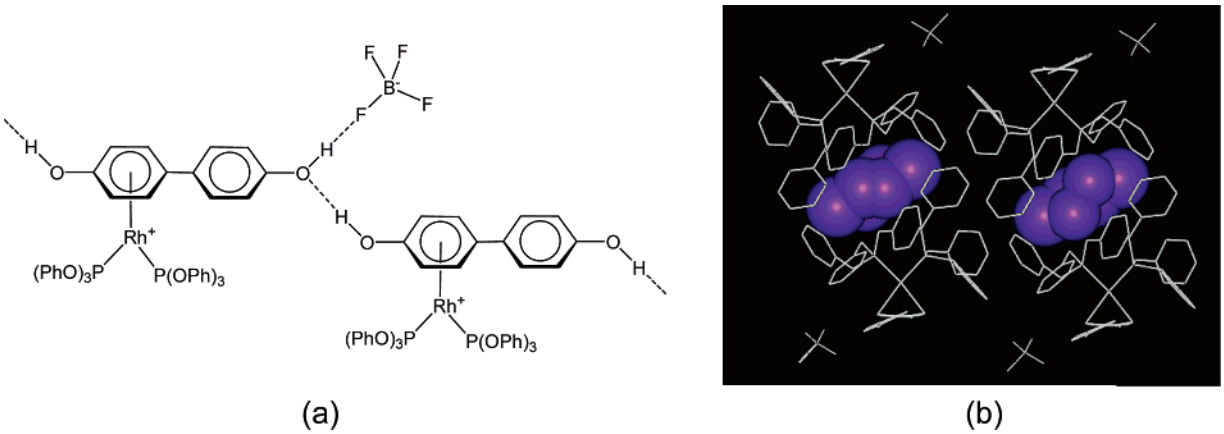

Figure 7. (a) 1-D hydrogen-bonded chain structure in $\mathbf{3}^{+}BF_4^{-}$. (b) Structure of $\mathbf{3}^{+}BF_4^{-}$ with disordered solvent (violet) in channels that are lined with phenyl rings.

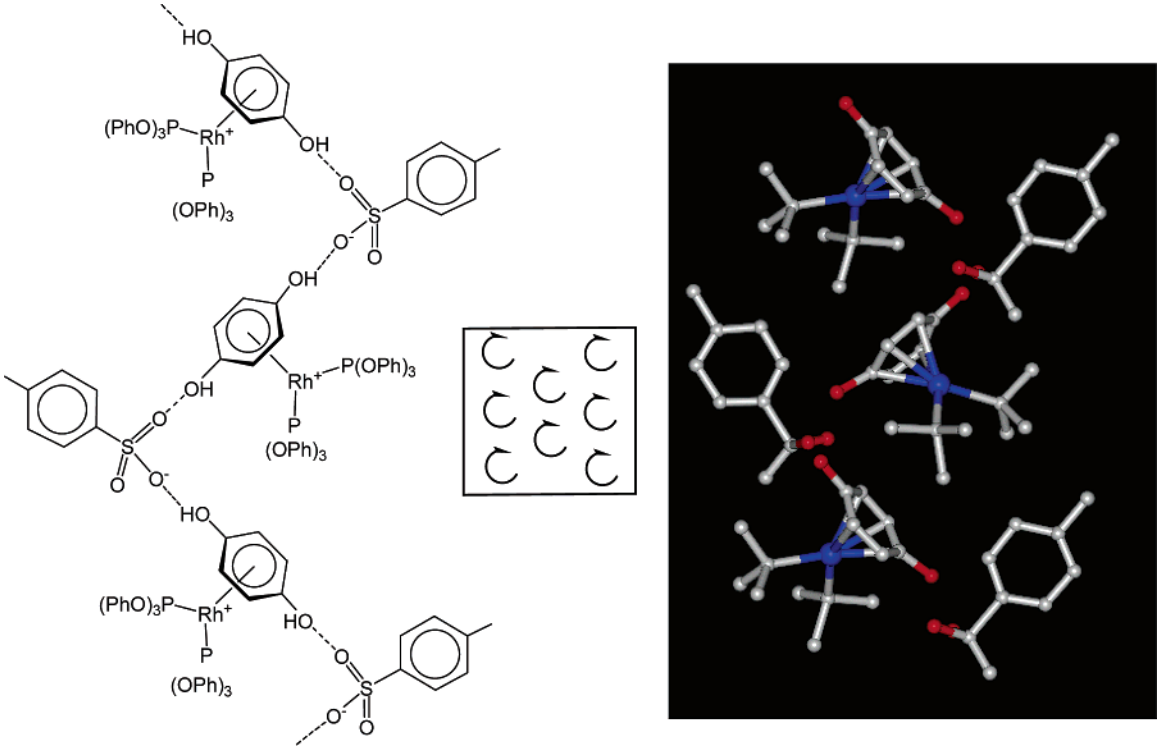

Figure 8. C_2-helical hydrogen-bonded structure found in $\mathbf{1}^+OTs^-$. The helices all pack with the same twist direction, resulting in a chiral crystal.

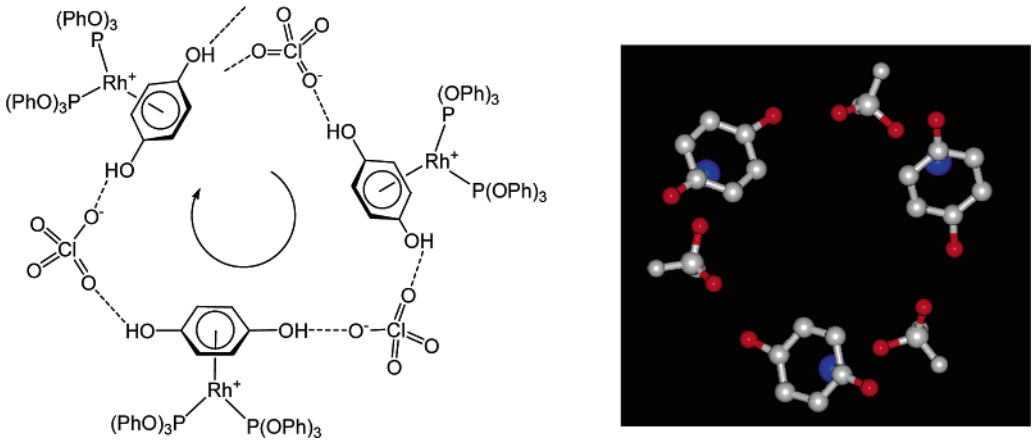

Figure 9. The C_3-helical hydrogen-bonded structure found in $\mathbf{1}^+ClO_4^-$ and $\mathbf{1}^+BF_4^-$.

Preliminary experiments were done to probe the possible interaction of appropriate aromatic molecules with the hydrophobic channels present in $\mathbf{1}^+ClO_4^-$ (Figure 10). As seen in Figure 12, the PXRD pattern of solid $\mathbf{1}^+ClO_4^-$ changes significantly after exposure to toluene for 5 days (Figure 12b) and then reverts to the original pattern after drying under vacuum. Although the details are unknown, it may be concluded that toluene interacts reversibly with the host channels in $\mathbf{1}^+ClO_4^-$.

Figure 13 shows TGA curves for $\mathbf{1}^+ClO_4^-$ and $\mathbf{1}^+BF_4^-$, along with curves for relevant tetrabutylammonium salts. A DSC experiment with $\mathbf{1}^+ClO_4^-$ showed the onset of a heat capacity change about 50 °C lower than the TGA decomposition temperature of ca. 180 °C. TGA experiments generally reflect gross thermal stability and not more subtle phase changes that may be occurring. It is suggested that the DSC result signals the breakup of the C_3-helical hydrogen-bonding assembly in $\mathbf{1}^+ClO_4^-$. The TGA curves show that there is not a great difference in the thermal stabilities of $\mathbf{1}^+ClO_4^-$ and $\mathbf{1}^+BF_4^-$. By comparison, $Bu_4N^+ClO_4^-$ and $Bu_4N^+BF_4^-$ decompose cleanly, with the tetrafluoroborate salt being more stable, as expected.

IR Studies and Atomic Charge Calculations. The hydrogen-bonding interactions between the organometallic cations and the counteranions shown in Chart 1 were studied in methylene chloride solution via FT-IR. The results are summarized in Figures14 and 15 and in Table 2. As shown in Figure 14, ν_{OH} in $\mathbf{1}^+$ is red-shifted by hydrogen bonding to the anion. With $\mathbf{1}^+SbF_6^-$, two IR peaks are seen at 3517 and 3405 cm^{-1} (labeled b and c). The peak at 3517 cm^{-1} is assigned to "free" $\mathbf{1}^+$: i.e., the complex not hydrogen-bonded to the counteranion. In support of this assertion, peak b also appears at the same frequency with the counterions BF_4^- and ClO_4^-. The much greater intensity of this peak in the case of SbF_6^- reflects the relatively poor ability of SbF_6^- to function as a hydrogen bond acceptor, a fact also indicated by the X-ray structures (vide supra).

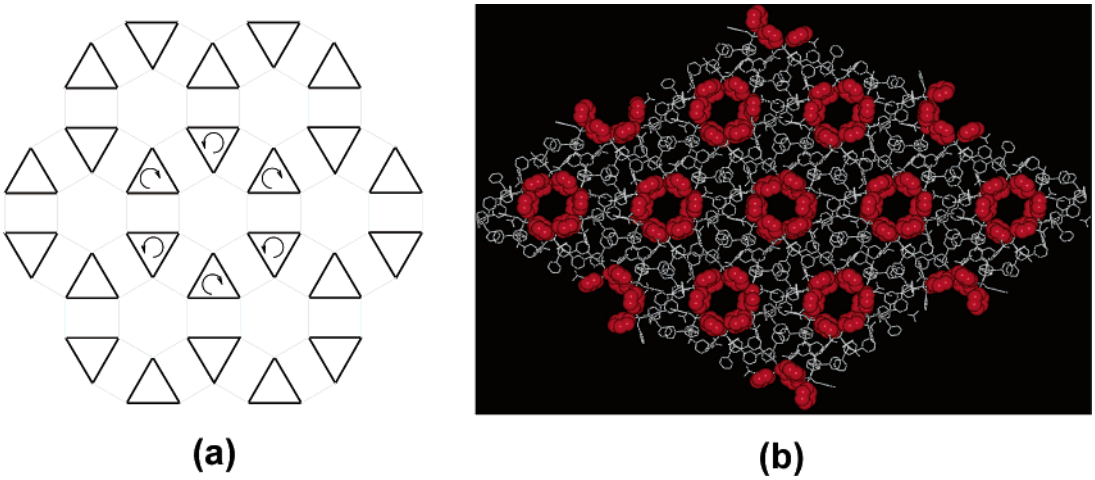

Figure 10. (a) 3-D packing of the C_3 helices in $\mathbf{1}^+ClO_4^-$ and $\mathbf{1}^+BF_4^-$. (b) Depiction of the resultant hydrophobic channels (red).

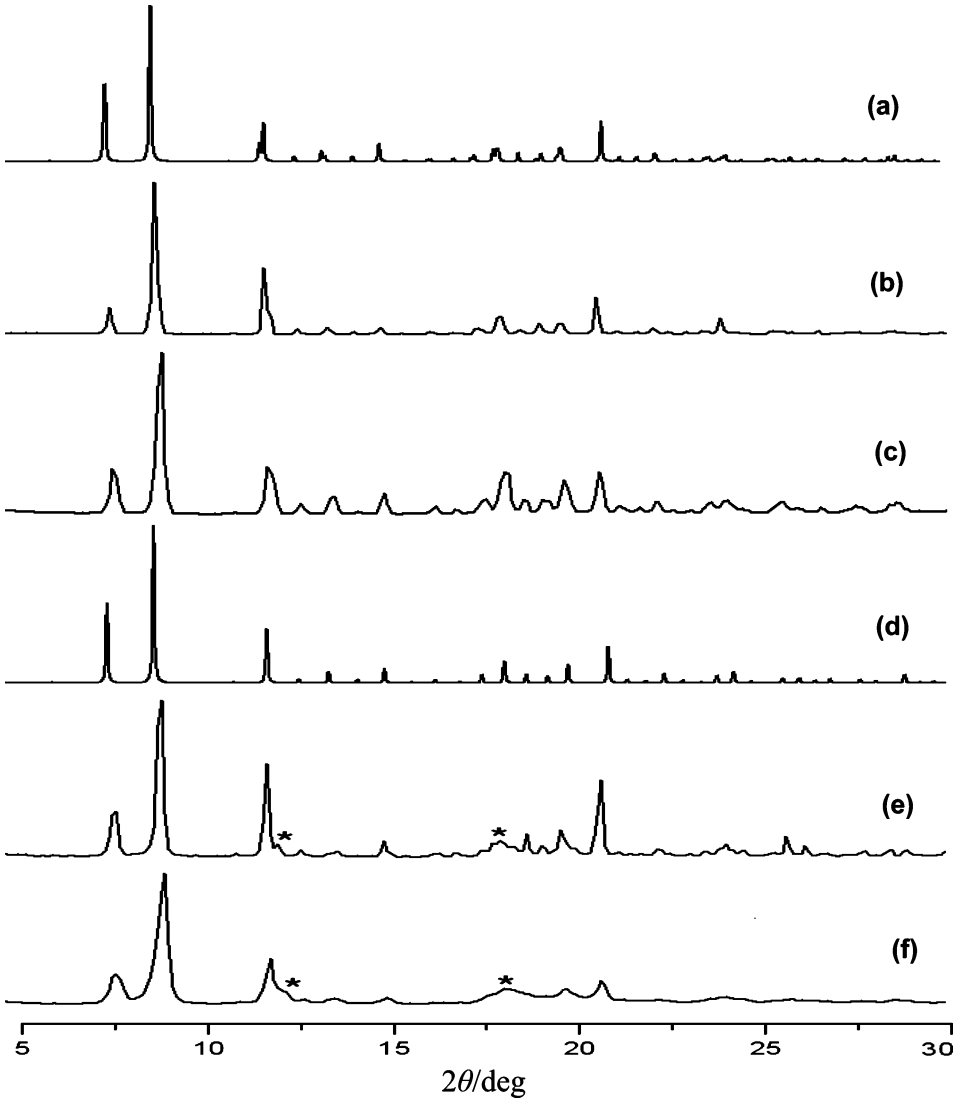

Figure 11. PXRD patterns: (a) simulated pattern of $\mathbf{1}^+ClO_4^-$ from single-crystal X-ray data; (b) experimental pattern of macrocrystals of $\mathbf{1}^+ClO_4^-$; (c) experimental pattern of microcrystals formed by simple precipitation of $\mathbf{1}^+ClO_4^-$; (d) simulated pattern of $\mathbf{1}^+BF_4^-$ from single-crystal X-ray data; (e) experimental pattern of macrocrystals of $\mathbf{1}^+BF_4^-$; (f) experimental pattern of microcrystals formed by simple precipitation of $\mathbf{1}^+BF_4^-$.

Peaks c−e in Figure 14 are assigned to hydrogen-bonded −OH groups. The shift of these ν_{OH} bands from the "free" position (peak b) can be used to estimate the strength of the H bonding between the hydroquinone −OH groups and the counterion by application of Iogansen's equation.[18] The results, presented in Table 2, indicate that H bonding between $\mathbf{1}^+$ or $\mathbf{2}^+$ and the counteranion is greater for O-based acceptors than for F-based acceptors. The hydrogen-bonding strength spans the

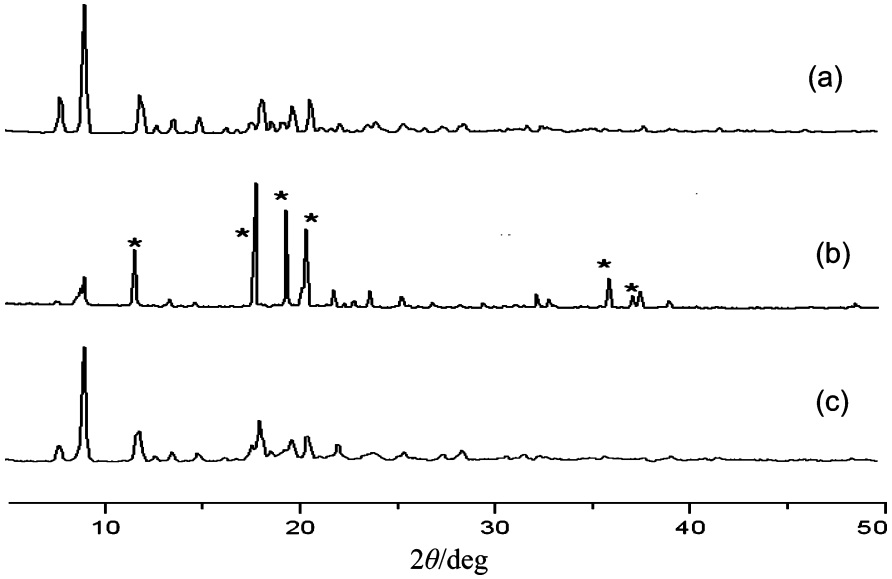

Figure 12. PXRD patterns: (a) $\mathbf{1}^+ClO_4^-$ freshly precipitated from methylene chloride with diethyl ether; (b) $\mathbf{1}^+ClO_4^-$ after exposure to neat toluene for 5 days; (c) $\mathbf{1}^+ClO_4^-$ after vacuum drying of sample in (b).

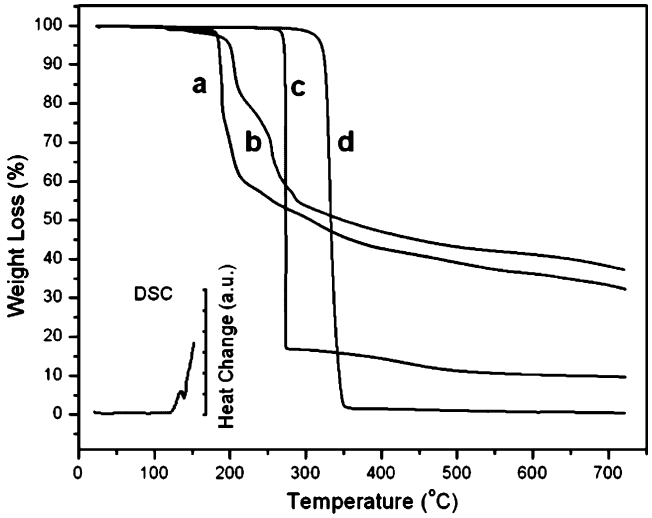

Figure 13. TGA curves: (a) $\mathbf{1}^+ClO_4^-$; (b) $\mathbf{1}^+BF_4^-$; (c) $Bu_4N^+ClO_4^-$; (d) $Bu_4N^+BF_4^-$. Inset is the DSC curve for $\mathbf{1}^+ClO_4^-$.

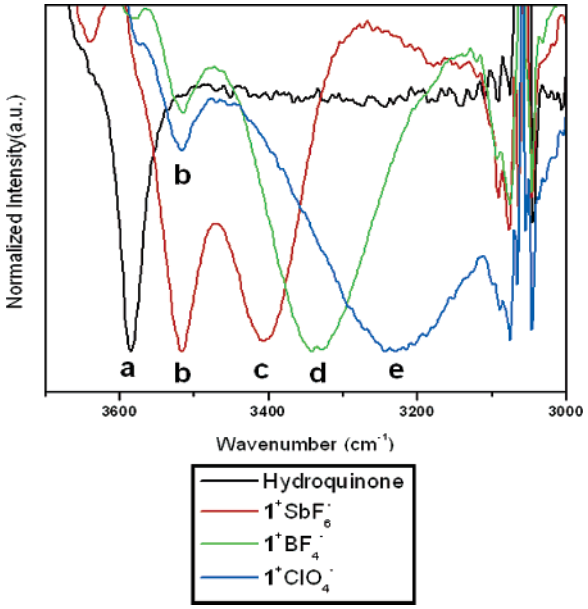

Figure 14. IR spectra in the ν_{OH} region (11 mM, CH_2Cl_2 solvent): (a) free 1,4-hydroquinone; (b) $\mathbf{1}^+X^-$ without hydrogen bonding between $\mathbf{1}^+$ and X^-; (c−e) $\mathbf{1}^+X^-$ with hydrogen bonding between $\mathbf{1}^+$ and X^-.

range 14−27 kJ/mol and follows the order $SbF_6^- < BF_4^- < ClO_4^- \leq OTf^- < OPf^-, OTs^-$.

The ν_{OH} bands in the IR spectra of free hydroquinone, resorcinol, and 4,4′-biphenol were found to be invariant over the concentration range utilized (3−11 mM), indicating the absence of intermolecular hydrogen bonding at these concentrations. In contrast, Figure 14 clearly shows that hydrogen bonding in $\mathbf{1}^+X^-$ can be extensive at 11 mM. The enhanced hydrogen bonding in $\mathbf{1}^+X^-$ can be attributed to (1) the positive charge on the cation brought about by the electrophilic rhodium fragment and (2) the obligatory anionic counterion that can act as a hydrogen bond acceptor. Charge pairing of the species in $\mathbf{1}^+X^-$ undoubtedly complements the hydrogen bonding. To probe the "charge-assisted" nature of the hydrogen bonding, IR spectra of CH_2Cl_2 solutions of 1,4-hydroquinone (11 mM) containing varying amounts of Bu_4ClO_4 were recorded. As shown in Figure 15, 1 equiv of Bu_4NClO_4 has little effect on the IR spectrum and, even with 10 equiv of Bu_4NClO_4 present, a significant amount of free hydroquinone remains. We conclude that the hydrogen bonding observed with $\mathbf{1}^+X^-$−$\mathbf{3}^+X^-$ has as important components both ionic charge pairing and electrophilic activation imparted by coordination to the transition metal.

Next, we performed molecular orbital calculations using Spartan[19] to assign atomic charges to the key terminal atoms for the range of counterions. Atomic charges are notoriously

(14) Quan, R. W.; Bercaw, J. E.; Schaefer, W. P. *Acta Crystallogr., Sect. C: Cryst. Struct. Commun.* **1991**, *C47*, 2057.
(15) Kannan, S.; James, A. J.; Sharp, P. R. *Inorg. Chim. Acta* **2003**, *345*, 8.
(16) X-ray structures of $\mathbf{1}^+BF_4^-$ and $\mathbf{2}^+BF_4^-$ were reported in ref 12.
(17) Charge-assisted hydrogen bonding of tosylate has been reported: Doubell, P. C. J.; Olivier, D. W.; Van Rooyen, R. H. *Acta Crystallogr., Sect. C: Cryst. Struct. Commun.* **1991**, *C47*, 353.
(18) The Iogansen equation is $\Delta H° = -1.28(\Delta\nu)^{1/2}$: (a) Kazarian, S. G.; Hamley, P. A.; Poliakoff, M. *J. Am. Chem. Soc.* **1993**, *115*, 9069. (b) Iogansen, G. A.; Kurkchi, G. A. Furman, V. M.; Glazunov, V. P.; Odinokov, S. E. *Zh. Prikl. Spektrosk.* **1980**, *33*, 460.
(19) Spartan '04, Version 1.0.3; Wavefunction, Inc., Irvine, CA 2004.

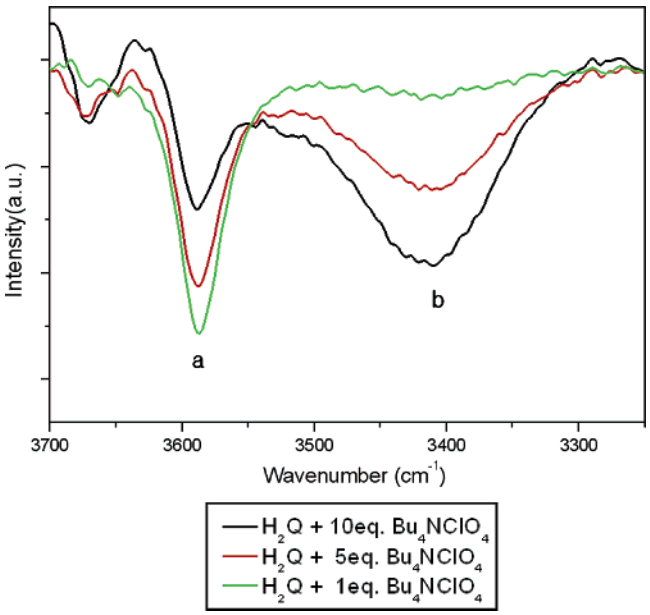

Figure 15. IR ν_{OH} peaks for 1,4-hydroquinone (H_2Q, 11 mM, CH_2Cl_2) in the presence of Bu_4NClO_4. Peak a is due to free H_2Q, and peak b is due to H_2Q hydrogen bonded to ClO_4^-.

Table 2. Summary of IR Study of Hydrogen Bonding[a]

	ν_{OH} (cm^{-1})			
compd	free	H bonded	shift	$-\Delta H^b$ (kJ/mol)
hydroquinone	3585[c]			
resorcinol	3580			
4,4′-biphenol	3598			
$\mathbf{1}^+ClO_4^-$	3517[d]	3231	286	21.6
$\mathbf{1}^+OTf^-$	3517[d]	3170	347	23.8
$\mathbf{1}^+OPf^-$	3517[d]	3078	439	26.8
$\mathbf{1}^+OTs^-$	3517[d]	3058	459	27.4
$\mathbf{1}^+BF_4^-$	3517[d]	3330	187	17.5
$\mathbf{1}^+SbF_6^-$	3517[d]	3405	112	13.5
$\mathbf{2}^+BF_4^-$	3505[d]	3321	184	17.4
$\mathbf{3}^+BF_4^-$	3573[e]	3296		

[a] Data obtained using 11 mM solutions in methylene chloride. [b] Calculated with the Iogansen equation.[18] [c] Peak unchanged in 3 mM solution. [d] ν_{OH} peak in coordinated hydroquinone, which is not hydrogen bonded. [e] The ν_{OH} peak in the uncoordinated phenol ring.

Table 3. Calculated Atomic Charges[a]

	SbF_6^-	BF_4^-	ClO_4^-	$CH_3C_6H_4SO_3^-$	$CF_3SO_3^-$		$PF_2O_2^-$	
	F	F	O	O	F	O	F	O
elec	−0.55	−0.55	−0.71	−0.81	−0.30	−0.76	−0.43	−0.90
mull	−0.49	−0.53	−0.66	−0.71	−0.42	−0.68	−0.47	−0.75
nat	−0.67	−0.61	−0.94	−1.08	−0.39	−1.06	−0.62	−1.13

[a] Using Spartan '04 with a 3-21G(*) Gaussian basis set. Abbreviations: elec, electrostatic potential; mull, Mulliken population analysis; nat, natural bond orbital population analysis.

difficult to define,[20] which led us to include the results from three differing approaches. However, regardless of the charge partitioning scheme used, the oxygen atoms are calculated to be more electron rich than the fluorine atoms (see Table 3). These results are in agreement with the observed preference for charge-assisted hydrogen bonding to oxygen over fluorine in OTf^- and OPf^-, as well as the trends observed in the IR spectra.

(20) Hehre, W. J. *A Guide to Molecular Mechanics and Quantum Chemical Calculations*; Wavefunction: Irvine, CA 2003; Chapter 16.

Conclusions

The organometallic salts [(η^6-hydroxybenzene)Rh(P(OPh)$_3$)$_2$]$^+X^-$ undergo noncovalent self-assembly dominated by charge-assisted hydrogen-bonding and $\pi-\pi$-stacking interactions. The electrophilic $Rh(P(OPh)_3)_2^+$ moiety activates the phenolic −OH groups to participate in strong hydrogen bonding to the anionic counterion X^-. The nature of the hydrogen-bonding interactions and the resulting 3-D structures are remarkably dependent on the identity of the anion. The X-ray structures of [(η^6-hydroquinone)Rh(P(OPh)$_3$)$_2$]X salts (X = BF_4, ClO_4, SbF_6, OTf, OTs, OPf) display an assortment of dimeric, C_2-helical, and C_3-helical motifs. This work demonstrates that self-assembly of well-designed organometallic building blocks via charge-assisted hydrogen bonding is an effective strategy for the construction of robust porous networks that are formed rapidly (minutes or less). With counterions containing both oxygen and fluorine, it was found that the former is invariably the hydrogen bond acceptor, a result in agreement with atomic charge calculations. It is anticipated that self-assembly via charge-assisted hydrogen bonding is an approach applicable to many organometallic systems.

Experimental Section

General Considerations: All reactions were carried out under N_2 in flame-dried glassware. HPLC-grade methylene chloride and diethyl ether solvents were used as received without further purification. $[Rh(COD)Cl]_2$ was provided by Strem Chemicals. The ^{1}H NMR spectra were recorded on Bruker (300 MHz) spectrometers. Elementary analyses were performed by Quantitative Technologies Inc. (QTI, Whitehouse, NJ). Thermogravimetric analyses (TGA, Q500 from TA Instruments) and differential scanning calorimetry (DSC, DuPont DSC 2910) were performed at scan rates of 5 and 10 °C/min using N_2, respectively. X-ray powder diffraction (PXRD) data were recorded on a Bruker D8 ADVANCE instrument at 40 kV and 40 mA with Cu Kα radiation (λ = 1.540 50 Å), a scan speed of 0.3°/s, and a step size of 0.1° in 2θ.

[(η^6-1,4-hydroquinone)bis(triphenyl phosphite)Rh]SbF_6-($\mathbf{1}^+\mathbf{SbF_6^-}$). After the glassware was flame-dried, $[Rh(P(OPh)_3)_2Cl]_2$[12] (0.36 g, 0.24 mmol) and $AgSbF_6$ (0.19 g, 0.56 mmol) were mixed for 1 h at room temperature in methylene chloride (5 mL). While the mixture was stirred, a white precipitate formed on the bottom of the glassware, after which 1,4-hydroquinone (0.10 g, 0.91 mmol) was added to the reaction mixture. After the mixture was stirred for 2 h at room temperature, the solvent was removed by rotary evaporation. The residue was dissolved in methylene chloride (3 mL) and slowly dropped into an ether solution through a Celite pad. A yellow solid formed in the ether solution and was collected by filtration (washed with diethyl ether, 10 mL, three times). The isolated yield was 83% (0.42 g, 0.39 mmol). Crystals were grown by dissolving $\mathbf{1}^+SbF_6^-$ (30 mg) in methylene chloride (1.0 mL) in a 5 mL vial and layering with 3 mL of diethyl ether. The solution was placed in a refrigerator for 2 weeks, after which yellow crystals formed on the wall of the vial. ^{1}H NMR (CD_2Cl_2): δ 7.37 (t, J = 7.8 Hz, OPh, 12H), 7.27 (t, J = 7.6 Hz, OPh, 6H), 7.03 (d, J = 7.8 Hz, OPh, 12H), 6.11 (br s, OH, 2H), 5.68 (s, hydroquinone ring, 4H). Anal. Calcd for vacuum-dried $C_{42}O_8H_{36}P_2RhSbF_6$: C, 47.18; H, 3.39. Found: C, 47.85; H, 3.48.

[(η^6-1,4-Hydroquinone)bis(triphenyl phosphite)Rh]OTf-($\mathbf{1}^+\mathbf{OTf^-}$). The same procedure was followed using AgOTf instead of $AgSbF_6$. The isolated yield was 91%. Crystals of $\mathbf{1}^+OTf^-$ were grown by layering a methylene chloride solution with hexane and cooling in a refrigerator for 2 days. Yellow crystals formed on the wall of the vial. ^{1}H NMR (CD_2Cl_2): δ 8.26 (br s, OH, 2H), 7.31(t, J = 8.0 Hz, OPh, 12H), 7.21 (t, J = 7.9 Hz, OPh, 6H), 6.97 (d, J

= 8.0 Hz, OPh, 12H), 5.47 (s, hydroquinone ring, 4H). Anal. Calcd for $C_{43}O_{11}H_{36}P_2RhSF_3$: C, 52.56; H, 3.69. Found: C, 53.08; H, 3.63.

[(η^6-1,4-Hydroquinone)bis(triphenyl phosphite)Rh]PF_2O_2 ($\mathbf{1}^+\mathbf{OPf}^-$). The same procedure was followed using $AgPF_6$ instead of $AgSbF_6$. Before recrystallization, the complex had PF_6^- as the counteranion. Anal. Calcd for $C_{42}O_8H_{36}P_3RhF_6$: C, 51.55; H, 3.71. Found: C, 52.04; H, 3.69. During recrystallization from methylene chloride, however, hydrolysis of the anion to $PF_2O_2^-$ (OPf^-) occurred to afford $\mathbf{1}^+OPf^-$ in a 66% isolated yield. ^{1}H NMR (CD_2Cl_2): δ 9.59 (br s, OH, 2H), 7.37(t, J = 8.0 Hz, OPh, 12H), 7.20 (t, J = 7.9 Hz, OPh, 6H), 6.98 (d, J = 8.0 Hz, OPh, 12H), 5.50 (s, hydroquinone ring, 4H). Anal. Calcd for $C_{42}O_{10}H_{36}P_3Rh_1F_2$: C, 53.98; H, 3.88. Found: C, 53.50; H, 3.73.

[(η^6-Resorcinol)bis(triphenyl phosphite)Rh]BF_4 ($\mathbf{2}^+\mathbf{BF_4}^-$). The synthesis and characterization of this compound are reported in ref 12.

[Rh(η^6-4,4-Biphenol)bis(triphenyl phosphite)]BF_4 ($\mathbf{3}^+\mathbf{BF_4}^-$). The same procedure was followed using 4,4-biphenol instead of hydroquinone. The isolated yield was 87%. Crystals of $\mathbf{3}^+BF_4^-$ were grown by layering a methylene chloride solution with hexane and cooling in a refrigerator for 3 days. Orange crystals formed on the wall of the vial. ^{1}H NMR (CD_2Cl_2): δ 8.39 (br s, OH, 1H), 7.26 (t, J = 7.5 Hz, OPh, 12H), 7.22 (t, J = 7.5 Hz, OPh, 6H), 6.90 (t, J = 7.6 Hz, OPh, 6H), 6.83 (d, J = 8.9 Hz, biphenol, 2H), 6.75(d, J = 6.75 Hz, biphenol, 2H), 6.00 (br s, OH, 1H), 5.92 (s, biphenol, 4H). Anal. Calcd for $C_{48}O_8H_{40}P_2RhBF_4$: C, 57.86; H, 4.05. Found: C, 57.74; H, 3.91.

[(η^6-1,4-Hydroquinone)bis(triphenyl phosphite)Rh]OTs-($\mathbf{1}^+\mathbf{OTs}^-$). The same procedure was followed using silver tosylate instead of $AgSbF_6$. The isolated yield was 95%. Crystals of $\mathbf{1}^+OTs^-$ were grown by layering a methylene chloride solution with hexane and cooling in a refrigerator for 3 days. ^{1}H NMR (CD_2Cl_2): δ 7.38 (d, J = 7.5 Hz, OTs, 2H), 7.27 (t, J = 7.8 Hz, OPh, 12H), 7.25 (d, J = 7.5 Hz, OTs, 2H), 7.15 (t, J = 7.6 Hz, OPh, 6H), 6.95 (d, J = 7.8 Hz, OPh, 12H), 6.69 (br s, OH, 2H), 5.55 (s, hydroquinone ring, 4H), 2.39 (s, OTs methyl, 3H). Anal. Calcd for $C_{50}O_{11}H_{43}P_2RhS$: C, 54.81; H, 3.94. Found: C, 54.66; H, 3.86.

[(η^6-1,4-Hydroquinone)bis(triphenyl phosphite)Rh]BF_4-($\mathbf{1}^+\mathbf{BF_4}^-$). The synthesis and characterization of this compound is reported in ref 12.

[(η^6-1,4-Hydroquinone)bis(triphenyl phosphite)Rh]ClO_4-($\mathbf{1}^+\mathbf{ClO_4}^-$). The same procedure was followed using $AgClO_4$ instead of $AgSbF_6$. The isolated yield was 79%. Crystals of $\mathbf{1}^+ClO_4^-$ were grown by layering a methylene chloride solution with hexane and cooling in a refrigerator for 4 days. ^{1}H NMR (CD_2Cl_2): δ 7.37(t, J = 7.9 Hz, OPh, 12H), 7.25 (t, J = 7.8 Hz, OPh, 6H), 7.01 (d, J = 7.8 Hz, OPh, 12H), 6.96 (br s, OH, 2H), 5.67 (s, hydroquinone ring, 4H). Anal. Calcd for $C_{42}O_{12}H_{36}P_2RhCl$: C, 54.07; H, 3.89. Found: C, 54.08; H, 4.01.

Single-Crystal X-ray Structure. X-ray data collection was carried out using a Bruker single-crystal diffractometer equipped with an APEX CCD area detector and controlled by SMART version 5.0 software. Collection was done at either 100 or 293 K. Data reduction was performed with SAINT version 6.0 software. The structures were generally determined by direct methods and refined on F^2 by use of programs in SHELXTL version 5.0. Most hydrogen atoms appeared in a difference map, or they were generally inserted in ideal positions, riding on the atoms to which they are attached.

Acknowledgment. S.U.S. is grateful for support by the Sungkyunkwan University Faculty Research Fund-2005. D.A.S. is pleased to acknowledge the donors of the Petroleum Research Fund, administered by the American Chemical Society, for support of this research.

Supporting Information Available: CIF files for all X-ray structures. This material is available free of charge via the Internet at http://pubs.acs.org. These files have also been deposited with the Cambridge Crystallographic Data Centre as registry numbers CCDC-299584−299590.

OM0604425